Magneto-Optical Investigations on the Formation and Dissociation of Intermolecular Charge-Transfer Complexes at Donor-Acceptor Interfaces in Bulk-Heterojunction Organic Solar Cells

ARTICLE *in* THE JOURNAL OF PHYSICAL CHEMISTRY B · APRIL 2010

Impact Factor: 3.3 · DOI: 10.1021/jp100241g · Source: PubMed

3 AUTHORS, INCLUDING:

Huidong Zang
Brookhaven National Laboratory
25 PUBLICATIONS **199** CITATIONS
SEE PROFILE

Zhihua Xu
Brookhaven National Laboratory
30 PUBLICATIONS **495** CITATIONS
SEE PROFILE

Magneto-Optical Investigations on the Formation and Dissociation of Intermolecular Charge-Transfer Complexes at Donor−Acceptor Interfaces in Bulk-Heterojunction Organic Solar Cells

Huidong Zang, Zhihua Xu, and Bin Hu*

Department of Materials Science and Engineering, University of Tennessee, Knoxville, Tennessee 37996

Received: January 11, 2010; Revised Manuscript Received: March 22, 2010

The electron−hole pairs can be formed in intermolecular charge-transfer (CT) states between two adjacent molecules due to Coulomb interaction in organic semiconducting materials. In general, the exciton dissociation can experience the intermediate states: intermolecular CT states at the donor−acceptor interfaces to generate a photocurrent in organic solar cells. This article reports the magneto-optical studies on intermolecular CT states in the generation of photocurrent by using magnetic field effects of photocurrent (MFE_{PC}) and light-assisted dielectric response (LADR). The MFE_{PC} and LADR studies reveal that internal electrical drifting and local Coulomb interaction can largely change the formation and dissociation of CT states by changing internal charge-transport channels and local Coulomb interaction through morphological development upon thermal annealing. Therefore, the MFE_{PC} and LADR can be used as effective magneto-optical tools to investigate charge recombination, separation, and transport in organic solar cells.

Introduction

Organic semiconducting polymers have become promising photovoltaic materials with large optical absorption coefficients, efficient formation of photoexcited states, and morphologically controllable charge-transport channels.[1–9] It has been experimentally found that the light absorption leads to the formation of Coulombically bound intramolecular electron−hole pairs, namely, Frenkel excitons with large binding energies in organic semiconducting polymers.[10–14] Therefore, sufficient donor−acceptor interaction is necessarily required to dissociate the photoexcited excitons for the generation of photocurrent in organic solar cells. In general, the dissociated electrons and holes can form electron−hole pairs at CT states in donor−acceptor interfaces due to intercharge Coulomb attraction.[15–19] As a result, dissociating electron−hole pairs at CT states is an important issue to improve photocurrent in organic solar cells.[20–24] In this article, we use magnetic field effects of photocurrents (MFE_{PC}) and light-assisted dielectric response (LADR) as new experimental tools to detect the electron−hole pairs in intermolecular CT states at the donor−acceptor interfaces. In particular, we investigate the effects of internal electrical drifting and local Coulomb interaction on the formation and dissociation of intermolecular CT states by adjusting morphological structures upon thermal annealing in the generation of photocurrents.

It is noted that the MFE_{PC} can be divided into low (<150 mT) and high (>150mT) field regimes corresponding to the dissociation processes in pristine polymers[25–27] and donor−acceptor bulk heterojunctions, respectively.[28–31] In general, the low-field MFE_{PC} from pristine polymers can show positive and negative components.[30,32–35] We have observed in our previous study[36] that MEH-PPV, which has nearly 100% singlets under photoexcitation, only shows a positive MFE_{PC} in the low-field regime. However, the P3HT, which has both significant singlet and triplet states under photoexcitation, gives both positive and negative components in the low-field MFE_{PC}. Therefore, we suggest that the positive and negative components in the low-field MFE_{PC} are due to singlets and triplets, respectively. It can be further suggested that the positive and negative components arise from the dissociation in polaron-pair states[32,33] and the charge reaction in excitonic states,[35–38] respectively. The positive MFE_{PC} generated by the dissociation of polaron pairs comes from the following two arguments. First, a low magnetic field can increase the singlet ratio in polaron-pair states through intersystem crossing by disturbing the spin momentum conservation involved in the intersystem crossing. Second, the singlets have stronger ionic natures in wave functions relative to the triplets due to different spin configurations and can therefore exhibit larger dissociation rates through the Onsager process in pristine conjugated polymers.[38–40] As a result, the dissociation in polaron-pair states can generate a positive component in low-field MFE_{PC} (Figure 1a). Indeed, the photoexcited excitons can Coulombically interact with charge carriers, generating an exciton-charge reaction. It can be suggested from the photophysics studies of radical pairs that the relevant outcome of the exciton-charge reaction is the separation of excitons to generate free charge carriers[35,41–45] (Figure 1a). Furthermore, magnetic field effects of electroluminescence have also suggested that the excitons can react with charge carriers with the consequence of generating free charges in organic light-emitting diodes.[43,46,47] It is noted that an external magnetic field can reduce the exciton-charge reaction rate constant,[35,38,48] leading to negative magnetic field effects in the generation of free charge carriers. Nevertheless, the negative low-field MFE_{PC} can indicate the existence of an exciton-charge reaction. It should be noted that the singlet and triplet excitons can dominate the dissociation of polaron pairs and the exciton-charge reaction, respectively, due to their different ionic natures and lifetimes. On the other hand, the high-field MFE_{PC} can be used as a new experimental tool to detect the electron−hole pairs formed in intermolecular CT states at donor−acceptor interfaces based on the following three fundamental arguments. First, the photophysics studies have suggested that the intermolecular CT states are formed with both singlet

* Corresponding author. E-mail: bhu@utk.edu.

10.1021/jp100241g
Published on Web 04/14/2010

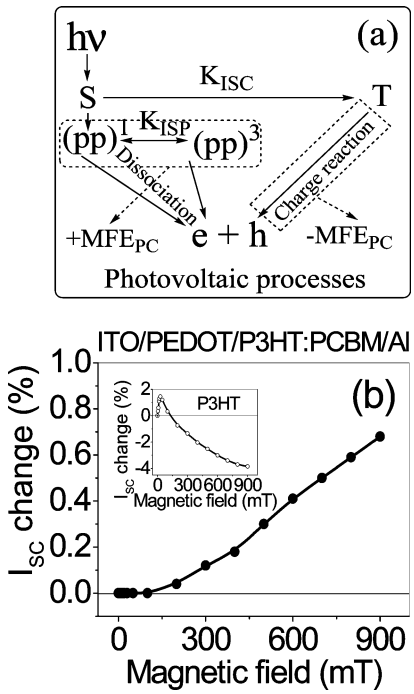

Figure 1. Photocurrent-generation channels in pristine semiconducting P3HT and magnetic field effects of photocurrent MFE_{PC} in the bulk-heterojunction P3HT:PCBM solar cell. (a) Photocurrent-generation channels: dissociation of polaron pairs, dominated by singlet excitons, and exciton-charge reaction, dominated by triplet excitons. S and T represent photoexcited singlet and triplet excitons. $(PP)^1$ and $(PP)^3$ are intermolecular singlet and triplet polaron pairs in pristine P3HT. K_{ISC} and K_{ISP} are intersystem crossing in excitonic and polaron-pair states. $+MFE_{PC}$ and $-MFE_{PC}$ are positive and negative components in magnetic field effects of photocurrent in low-field regimes. (b) MFE_{PC} for ITO/PEDOT/P3HT:PCBM/Al solar cell. The weight ratio of P3HT:PCBM is 1:0.8. The MFE_{PC} for the pristine P3HT device (ITO/P3HT/Al) is shown as an inset.

and triplet states through geminate and nongeminate capture of dissociated electrons and holes at donor−acceptor interfaces when electron spin multiplicities are considered.[49] Second, an external magnetic field can change the singlet and triplet ratios in the intermolecular CT states by perturbing the intersystem crossing[32,38,50] through spin momentum conservation. Third, the singlet and triplet intermolecular CT states can have high and low dissociation rates in bulk heterojunctions,[40,51] respectively, similar to polaron pairs in pristine polymers due to their different ionic natures involved in dissociation driven by the Onsager process.[39] Therefore, applying an adequate magnetic field can change the photocurrent by altering the singlet and triplet ratios in CT states, generating high-field MFE_{PC} in bulk-heterojunction organic solar cells.[30,31,52] Furthermore, we found that light-assisted dielectric response (LADR) can provide experimental information on charge generation, transport, and collection in donor and acceptor interpenetrating networks when an organic solar cell is operated in capacitor mode under photoexcitation. Specifically, the measurement of device capacitance under light illumination can essentially reflect the following three pieces of information. First, the local electrical polarizabilities from the Coulomb interaction can be given under dark conditions when light illumination is off. Second, at a given light illumination, the capacitance change caused by light illumination can be related to the generation of charge carriers. Third, the measurement of device capacitance with light illumination can describe the transport of generated charge carriers. Therefore, the use of MFE_{PC} and LADR can reveal the internal photovoltaic processes in bulk-heterojunction organic solar cells.

Experimental Section

The regioregular poly(3-hexylthiophene) (P3HT) and fullerene derivative 1-(3-methyloxycarbonyl)-propyl-1-phenyl (6,6) C_{61} (PCBM) were purchased from Aldrich and American Dye Sources, Inc., respectively. The number-average molecular weight M_n of P3HT is 87 000. The P3HT:PCBM composite films were spin-cast from chrolobenzene solutions with the thickness of 80 nm on indium−tin−oxide (ITO) glass substrates precoated with a 40 nm thin layer of poly(3,4-ethylenedioxythiophene):poly(styrene sulfonate) (PEDOT:PSS) (Baytron P 4083) in nitrogen atmosphere. The P3HT:PCBM compositions are given by their relative weight ratios. The bulk-heterojunction organic solar cells were then fabricated by the vacuum deposition of aluminum (Al) electrode with the device architecture of ITO/PEDOT/P3HT:PCBM/Al. Thermal annealing was carried out in nitrogen atmosphere by thermally heating the devices with selected temperature and time period. The MFE_{PC} and LADR measurements were performed based on a single device with continuous thermal annealing starting from low to high temperatures to remove experimental errors. The double-layer solar cells were also fabricated by using TiOx and ZnO films, as more and less polar materials, with a P3HT layer. The TiOx and ZnO films were prepared by spin-casting with the thickness of 60 nm from their respective solutions based on published procedures.[53,54] The thickness of the P3HT layer was controlled at 80 nm in the double-layer devices. The photocurrent−voltage characteristics were measured by using the Keithley 2400 source meter and the photoillumination of AM1.5G 100 mW/cm^2 from the Thermal Oriel 96000 300 W solar simulator for the fabricated solar cells. The MFE_{PC} was measured from the solar cells placed in a magnetic field under light illumination with a central wavelength of 500 nm selected by a monochromator and transported through a liquid light waveguide fiber. The magnetic field was applied parallel to the device plane during measurements. However, the MFE_{PC} does not show appreciable angle dependence with magnetic field direction in the P3HT:PCBM bulk-heterojunction solar cells. The MFE_{PC} is determined by the relative change in photocurrent at short-circuit conditions: $(I_{(B)} - I_{(0)})/(I_{(0)})$, where $I_{(B)}$ and $I_{(0)}$ are the photocurrents with and without a magnetic field. The light-assisted dielectric response LADR was recorded by using a dielectric spectrometer (Agilent, E4980A) to measure the capacitance of bulk-heterojunction organic solar cells. Specifically, the capacitance measurement was performed for organic solar cells under light illumination from a sunlight simulator. The light illumination intensity was changed by using different neutral optical filters. The LADR results were obtained by measuring the capacitance of the bulk-heterojunction solar cell with light illumination intensity. The photoluminescence (PL) was characterized by using a SPEX Florolog 3 spectrometer. All measurements were performed in a nitrogen gas atmosphere at room temperature.

Results and Discussion

Figure 1(b) shows the MFE_{PC} for the P3HT:PCBM bulk-heterojunction solar cell when the short-circuit photocurrent was measured as a function of magnetic field. Clearly, the P3HT:PCBM bulk-heterojunction solar cell lacks a low-field MFE_{PC} (<150 mT) but shows a considerable high-field MFE_{PC} (>150 mT). Specifically, the MFE_{PC} remains flat at low field (0 ∼ 150 mT) but has a positive component at high field (150 mT ∼ 1 T). On contrast, the pristine P3HT device shows a significant low-field MFE_{PC} with typical rapid increase and slow decrease components based on a short-circuit photocurrent. However, the pristine P3HT does not exhibit a positive high-field MFE_{PC}.

Therefore, we can suggest that the low-field and high-field MFE_{PC} can be attributed to pristine organic semiconducting materials and bulk heterojunctions, respectively. In the pristine P3HT device, the positive and negative low-field MFE_{PC} indicate that the photocurrent is generated by two processes: the dissociation of polaron pairs and the charge reaction in excitonic states. In contrast, the lack of low-field MFE_{PC} implies that the strong donor−acceptor interaction can directly dissociate both singlet and triplet excitons without going through polaron-pair states and the exciton-charge reaction process and consequently removes the low-field MFE_{PC} in the P3HT:PCBM solar cell. In particular, the positive high-field MFE_{PC} implies that the exciton dissociation undergoes significant CT states at donor−acceptor interfaces in bulk heterojunctions.[36] Especially, the dissociation of CT states generates a positive signal in high-field MFE_{PC}. This positive high-field MFE_{PC} generated by the CT states is similar to the positive low-field MFE_{PC} generated by the polaron pairs. This similarity can be attributed to the fact that both polaron pairs and CT states are electron−hole pairs. Specifically, a polaron pair is formed when the electron and hole are captured in different molecules in pristine polymers, while a CT state is generated when an electron and hole are captured at the donor and acceptor interface in bulk heterojunctions. Therefore, both polaron pairs and CT states are essentially electron−hole pairs. However, the electron−hole separation distance in CT states is usually shorter than that in polaron pairs due the close contact between donor and acceptor domains in bulk heterojunctions. Due to the shorter electron−hole separation distance, CT states can have larger binding energies and exchange energies relative to polaron pairs. We should note that bulk heterojunctions are still more efficient to generate a photocurrent although the CT states have larger binding energies. This is because (i) almost every exciton undergoes dissociation; (ii) the donor and acceptor interpenetrating networks can largely facilitate the charge collection at respective electrodes; and (iii) only a portion of dissociated charge carriers forms the CT states at donor and acceptor interfaces in bulk heterojunctions. On contrast, only a small portion of excitons undergo dissociation to form polaron pairs in pristine polymers. In addition, pristine polymers lack sufficient donor and acceptor interpenetrating networks for the collection of dissociated charge carriers. As a consequence, pristine polymers are not efficient to generate photocurrent, although the polaron pairs have lower binding energies.

We further examined the relationship between positive high-field MFE_{PC} and CT states by using double-layer design with different dielectric materials: TiOx and ZnO, respectively. The TiOx and ZnO have different dielectric constants ($\varepsilon \approx 86$ for TiOx, $\varepsilon \approx 8$ for ZnO)[55] but similar electronic levels (LUMO = 4.4 eV and HOMO = 8.1 eV for TiOx;[8] LUMO = 4.3 eV and HOMO = 7.7 eV for ZnO[56]). In particular, TiOx and ZnO can be used as more and less polar materials to form the double-layer solar cells with the P3HT. Figure 2(a) shows that the use of a more polar TiOx layer causes a positive high-field MFE_{PC}. On contrast, the less polar ZnO layer does not appreciably change the MFE_{PC} from the P3HT, lacking high-field MFE_{PC}. In addition, the P3HT/TiOx solar cell shows a larger photocurrent and photoluminescence (PL) quenching relative to the P3HT/ZnO device (Figure 2(b)). The larger PL quenching caused by the TiOx film can be attributed to the stronger Coulomb interaction between P3HT and TiOx at the interface due to the larger dielectric constant from the TiOx. Nevertheless, these experimental results imply that (i) more polar TiOx can enhance the exciton dissociation through local Coulomb interaction and (ii) the dissociated electrons and holes form CT states at the P3HT/TiOx interface in the generation of photocurrent in the double-layer organic solar cell. Therefore, the comparison between more and less polar effects in MFE_{PC} further indicates that the high-field MFE_{PC} can be attributed to the electron−hole pairs formed in CT states and the donor−acceptor interfaces in organic solar cells. We should note that the MFE_{PC} signal from the CT states in the P3HT/TiOx covers both low- and high-field regimes, while the MFE_{PC} signal from the CT states in the P3HT:PCBM bulk heterojunctions only exists in high-field regimes. This is because the MFE_{PC} signal consists of the contributions from both bulk and interface in the P3HT/TiOx device, and the combination of bulk (low-field positive and negative components) and interface (high-field positive component) contributions can produce a positive MFE_{PC} covering low- and high-field regimes. For the P3HT:PCBM bulk heterojunctions, the MFE_{PC} signal only consists of the contribution from the CT states formed at the donor and acceptor interfaces and consequently gives rise to a positive component at high field.

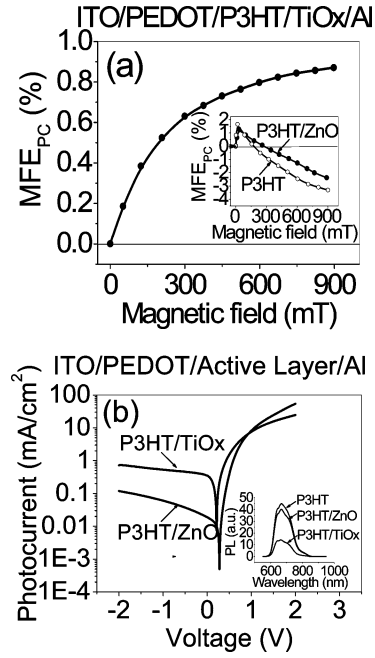

Figure 2. Magnetic field effects of photocurrent (MFE_{PC}), short-circuit current−voltage ($I_{SC}-V$), and PL quenching for P3HT/TiOx and P3HT/ZnO double-layer solar cells. (a) MFE_{PC} for ITO/PEDOT/P3HT/TiOx/Al solar cell. The MFE_{PC} for ITO/PEDOT/P3HT/ZnO/Al and ITO/PEDOT/P3HT/Al are shown as insets. (b) $I_{SC}-V$ for P3HT/TiOx and P3HT/ZnO double-layer solar cells. Inset: PL quenching for P3HT with TiOx and ZnO dielectric films, respectively, in double-layer design.

The experimental studies from transient absorption measurements have suggested that the formation of an electron−hole pair in CT states is determined by the competition between the free energy of charge separation and the Coulomb binding energy.[20] On the basis of this experimental finding, we can consider the electrically attractive force F_A, due to the Coulomb interaction, and the electrical drifting force F_D, due to the built-in electric field in the formation of electron−hole pairs in CT states, as schematically shown in Figure 3. The Coulomb interaction depends on both dielectric constant ε in the medium and the electron−hole separation distance at donor−acceptor interfaces. The built-in electric field can be estimated by the open-circuit voltage V_{OC}, given by $E = V_{OC}/D$, where D is the photovoltaic film thickness. The total energy U of a CT state can therefore consist of electronic energy associated with donor

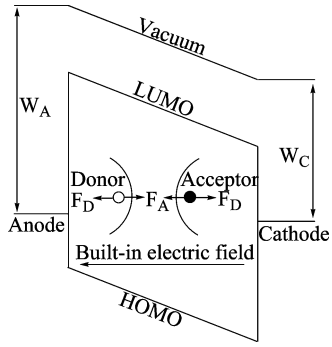

Figure 3. Schematic for intermolecular CT states formed at donor−acceptor interfaces under the competition between Coulombic attraction (F_A) and electrical drifting (F_D) force. W_A and W_C are the workfunctions for the anode and cathode.

and acceptor electronic levels, potential energy from the Coulomb attraction, and kinetic energy from electrical drifting (eq 1).

$$U = |E_D(\mathrm{HOMO}) - E_A(\mathrm{LUMO})| - \frac{1}{4\pi\varepsilon}\frac{e^2}{r} + \frac{1}{2}m_e v_e^2 + \frac{1}{2}m_h v_h^2 \quad (1)$$

where E_D(HOMO) and E_A(LUMO) are the HOMO for donor and the LUMO for acceptor; v_e and v_h are the electron and hole drifting velocities; m_e and m_h are the masses for electron and hole; r is the separation distance between electron and hole at the donor−acceptor interface; and ε is the medium dielectric constant. It can be seen from eq 1 that increasing the kinetic energy can reduce the stability of charge-transfer complexes and consequently enhance the dissociation of CT states. However, increasing the Coulomb potential energy can stabilize the CT states and thus weaken the dissociation of CT states. In principle, changing the potential energy, through Coulomb interaction, and the kinetic energy, through electrical drifting, forms a mechanism to control the formation and dissociation of CT states at the donor−acceptor interfaces in organic solar cells. In potential energy, the medium dielectric constant and donor−acceptor interfacial distance essentially determine the electron−hole capture probability in the formation of CT states through Coulomb interaction. In kinetic energy, the built-in electric field and charge mobility control the probability for dissociated electrons and holes to completely escape from their mutual Coulomb attraction toward the generation of photocurrent. Therefore, adjusting kinetic and potential energies through electrical drifting and Coulomb interaction can essentially change the density of intermolecular CT states.

Figure 4(a) shows that the morphological adjustment through thermal annealing can reduce the high-field MFE_{PC} signal strength in the P3HT:PCBM (1:0.8) solar cell. According to the high-field signal amplitude at 900 mT, the optimized thermal annealing (five-minute heating at 155 °C) can largely decrease the density of CT states by at least 61% in the ITO/PEDOT/P3HT:PCBM/Al solar cell (Figure 4(a)). The transient spectroscopy measurements have found that thermal annealing can significantly increase the yield of dissociated charge carriers by increasing the free energy of charge separation.[57] Our studies of high-field MFE_{PC} have further shown that the thermal annealing can also reduce the density of CT states in P3HT:PCBM bulk-heterojunction solar cells through morphological development. We note in the formation of CT states that the

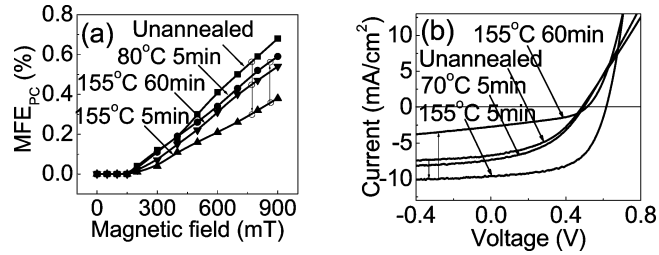

Figure 4. High-field MFE_{PC} and photocurrent current−voltage ($I_{SC}-V$) characteristics for the ITO/PEDOT/P3HT:PCBM(1:0.8)/Al device with continuous thermal annealing staring from low to high temperatures. (a) High-field MFE_{PC}. (b) $I_{SC}-V$ characteristics.

electron and hole drifting velocities v_e and v_h involved in the kinetic energy depend on both charge mobility and built-in electric field, given by

$$v_e = \mu_e \cdot E$$
$$v_h = \mu_h \cdot E \quad (2)$$

where μ_e and μ_h are the electron and hole mobilities and E is the built-in electric field. It has been experimentally found that thermal annealing can substantially improve the interpenetrating networks for charge transport[58–60] and consequently increases charge mobilities.[57,61–64] It can therefore be suggested from eq 2 that the increase in charge mobilities upon annealing can lead to a reduction in the density of CT states through increasing kinetic energies of dissociated electrons and holes in organic solar cells. In addition, the earlier experimental studies have already found that thermal annealing can significantly improve photovoltaic efficiencies of the P3HT:PCBM solar cells[6,59,65–67] due to the improvements of optical absorption and charge mobilities induced by morphological change through PCBM aggregation and P3HT chain packing caused by thermal annealing.[58,60,67–70] Figure 4(b) indicates that the power conversion efficiency (PCE) was improved from 1.4% for the unannealed device (I_{SC} = 6.5 mA/cm^2, V_{OC} = 0.49 V, FF = 0.42) to 3.5% for the optimally annealed device (I_{SC} = 9.6 mA/cm^2, V_{OC} = 0.61 V, FF = 0.60) under the simulated sunlight illumination of 100 mW/cm^2 (AM1.5). Our MFE_{PC} results suggest that the reduction in the density of CT states can also contribute to the improvement of photovoltaic efficiencies upon thermal annealing.

Now we discuss the binding energy and dissociation of CT states formed at donor−acceptor interfaces in organic solar cells based on the experimental measurements of electrical field dependence of MFE_{PC}. It was observed that the MFE_{PC} can be significantly increased in organic solar cells by reducing the dissociation of photoexcited states around open-circuit conditions when a forward electric field is applied to cancel the internal electric field.[27] This experimental result implies that the density of photoexcited states responsible for MFE_{PC} can be modulated by the external electric field through a dissociation process. Here, we apply a reverse electric field to enhance the dissociation of CT states and consequently to decrease the MFE_{PC} amplitude. We should note that the measurement of MFE_{PC} versus reverse electric field can provide the information on the binding energy of CT states. Figure 5(a) shows that an applied reverse electric field can decrease the high-field MFE_{PC} signal in the annealed P3HT:PCBM (1:0.8) solar cell. The amplitude reduction of high-field MFE_{PC} at 900 mT shows that the applied electric field of 2.0 V reverse bias reduces the density of CT states by 18% in the annealed P3HT:PCBM solar cell.

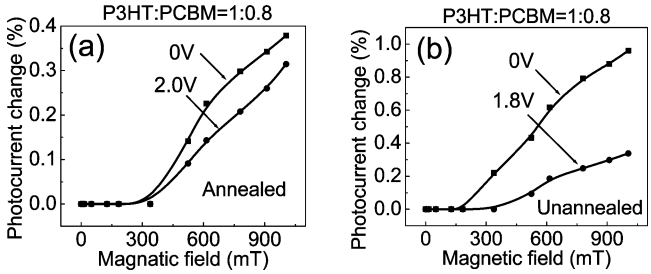

Figure 5. Applied electric field effects on high-field MFE_{PC} for the ITO/PEDOT/P3HT:PCBM (1:0.8)/Al solar cells before and after annealing. (a) Annealed solar cell. (b) Unannealed solar cell. The equivalent electric fields were applied by using reverse biases of 2.0 V (after annealing) and 1.8 V (before annealing).

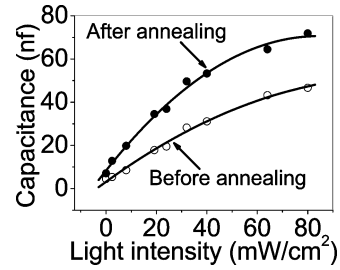

Figure 6. Light-assisted dielectric response is shown for the P3HT:PCBM bulk-heterojunction solar cell before and after annealing, respectively. The capacitance is plotted as a function of light illumination intensity when the P3HT:PCBM solar cell is operated in capacitor mode.

This experimental result indicates that the applied external electric field can compete with the electron−hole Coulomb attraction in the CT states and consequently decreases the density of CT states by enhancing the dissociation of CT states at the donor−acceptor interfaces. It should be further noted that the unannealed P3HT:PCBM solar cell shows a much larger reduction (∼65%) in the high-field MFE_{PC} signal amplitude under the influence of an equivalent applied electric field (1.8 V reverse bias) (Figure 5(b)). This experimental result implies that thermal annealing can indeed destroy the CT states of lower binding energy. However, the CT states with higher binding energy still exist after thermal annealing. In addition, it can also be seen that the annealed device shows a higher threshold (∼300 MT) in the MFE_{PC} as compared to the unannealed device (threshold ∼180 mT). This implies that the remaining CT states have larger exchange energies in the annealed P3HT:PCBM solar cell. It can be suggested from the larger exchange energies that thermal annealing enhances the donor and acceptor interfacial contacts and consequently reduces the donor and acceptor separation distance for more efficient dissociation. Clearly, the thermal annealing can dissociate low binding-energy CT states and significantly reduce the total density of CT states by enhancing the kinetic energies of dissociated charge carriers (eq 1). However, the remaining CT states have higher binding energies at the donor and acceptor interfaces in the annealed P3HT:PCBM solar cell. On the other hand, the unannealed P3HT:PCBM solar cell has lower binding energies but higher density of CT states. Therefore, completely removing the CT states is an important issue in the generation of photocurrent in bulk-heterojunction solar cells. It can be suggested from eq 1 that the internal charge transport and local Coulomb interaction are two critical parameters that control the formation of CT states at donor−acceptor interfaces. Here, we use light-assisted dielectric response (LADR) to investigate the charge transport and local Coulomb interaction upon thermal annealing when the P3HT:PCBM solar cell is operated in capacitor mode under photoexcitation. Figure 6 shows the capacitance of the P3HT:PCBM solar cell as a function of light illumination intensity before and after annealing. It is known that the capacitance is essentially related to the internal electrical polarization of the P3HT:PCBM blend film and the amount of photogenerated charge carriers stored in the electrodes in the P3HT:PCBM solar cell. It can be seen from Figure 6 that the thermal annealing causes three changes in the dielectric response. First, under dark condition the device capacitance slightly increases with thermal annealing in the P3HT:PCBM solar cell. This indicates that the thermal annealing increases the electrical polarizabilities of local morphological structures through P3HT chain packing and PCBM aggregation and consequently enhances the overall dielectric constant of P3HT:PCBM film. It should also be noted that our experimental result of enhanced dielectric constant can explain the early published result: the increase of absorbance for P3HT:PCBM film after thermal annealing.[61,64] Moreover, this morphology-dependent polarizability can be backed by nanosize-dependent dielectric interaction in nanomaterials.[71,72] It has been suggested that the increased electrical polarizabilities can increase the donor−acceptor interaction and thus reduce the formation of CT states.[73] Second, at a given light illumination intensity the thermal annealing increases the device capacitance in the P3HT:PCBM solar cell. This result implies that the thermal annealing can indeed increase the exciton dissociation and consequently the amount of photocharge carriers stored in the respective electrodes through morphological development. Third, the larger increase in rate of device capacitance with light illumination intensity implies that the thermal annealing enhances the charge-transport channels for dissociated electrons and holes to drift to respective electrodes. It is noted that the enhancement of charge-transport channels can essentially decrease the stability of CT states by increasing the kinetic energies of dissociated electrons and holes at the donor−acceptor interfaces. Nevertheless, the light-assisted dielectric studies reveal that morphological development generates three outcomes upon thermal annealing: (i) the increase of electrical polarizations of local P3HT and PCBM morphological structures, (ii) the increase in effective donor−acceptor interaction and exciton dissociation, and (iii) enhancement of charge-transport channels.

Conclusion

In summary, our magneto-optical studies indicate that MFE_{PC} and LADR can present as new experimental tools to investigate the intermolecular CT states at donor−acceptor interfaces during exciton dissociation in the generation of photocurrent in bulk-heterojunction organic solar cells. The MFE_{PC} and LADR measurements have shown that morphological development can change the internal electrical drifting and local Coulomb interaction and consequently affect the formation and dissociation of CT states at the donor−acceptor interfaces in the generation of photocurrent in bulk-heterojunction organic solar cells. Specifically, the competition between electrical drifting force and Coulomb attraction determines the formation and dissociation probabilities of electron−hole pairs in the CT states at the donor−acceptor interfaces. As a result, adjusting internal electrical drifting and local Coulomb interaction through materials design and film-morphological development presents a fundamental pathway to improve the photocurrent by controlling the formation and dissociation of intermolecular CT states at the donor−acceptor interfaces in bulk-heterojunction organic solar cells.

Acknowledgment. This research was supported by the Sustainable Energy Education and Research Center and the

Center for Materials Processing at the University of Tennessee. This research was partially conducted at the Center for Nanophase Materials Sciences, which is sponsored at Oak Ridge National Laboratory by the Division of Scientific User Facilities, U.S. Department of Energy.

References and Notes

(1) Sariciftci, N. S.; Smilowitz, L.; Heeger, A. J.; Wudl, F. *Science* **1992**, *258*, 1474.
(2) Yu, G.; Gao, J.; Hummelen, J. C.; Wudl, F.; Heeger, A. J. *Science* **1995**, *270*, 1789.
(3) Granstrom, M.; Petritsch, K.; Arias, A. C.; Lux, A.; Andersson, M. R.; Friend, R. H. *Nature* **1998**, *395*, 257.
(4) Shaheen, S. E.; Brabec, C. J.; Sariciftci, N. S.; Padinger, F.; Fromherz, T.; Hummelen, J. C. *Appl. Phys. Lett.* **2001**, *78*, 841.
(5) Xue, J. G.; Uchida, S.; Rand, B. P.; Forrest, S. R. *Appl. Phys. Lett.* **2004**, *84*, 3013.
(6) Li, G.; Shrotriya, V.; Huang, J. S.; Yao, Y.; Moriarty, T.; Emery, K.; Yang, Y. *Nat. Mater.* **2005**, *4*, 864.
(7) Zhang, F. L.; Mammo, W.; Andersson, L. M.; Admassie, S.; Andersson, M. R.; Inganas, L.; Admassie, S.; Andersson, M. R.; Ingands, O. *Adv. Mater.* **2006**, *18*, 2169.
(8) Kim, J. Y.; Lee, K.; Coates, N. E.; Moses, D.; Nguyen, T. Q.; Dante, M.; Heeger, A. J. *Science* **2007**, *317*, 222.
(9) Huang, F.; Chen, K.-S.; Yip, H.-L.; Hau, S. K.; Acton, O.; Zhang, Y.; Luo, J.; Jen, A. K. Y. *J. Am. Chem. Soc.* **2009**, *131*, 13886.
(10) Brédas, J.-L.; Cornil, J.; Heeger, A. J. *Adv. Mater.* **1996**, *8*, 447.
(11) Rand, B. P.; Burk, D. P.; Forrest, S. R. *Phys Rev B* **2007**, *75*, 115327.
(12) Blinov, L. M.; Palto, S. P.; Ruani, G.; Taliani, C.; Tevosov, A. A.; Yudin, S. G.; Zamboni, R. *Chem. Phys. Lett.* **1995**, *232*, 401.
(13) Alvarado, S. F.; Seidler, P. F.; Lidzey, D. G.; Bradley, D. D. C. *Phys. Rev. Lett.* **1998**, *81*, 1082.
(14) Osterbacka, R.; Wohlgenannt, M.; Shkunov, M.; Chinn, D.; Vardeny, Z. V. *J. Chem. Phys.* **2003**, *118*, 8905.
(15) Ohkita, H.; Cook, S.; Astuti, Y.; Duffy, W.; Tierney, S.; Zhang, W.; Heeney, M.; McCulloch, I.; Nelson, J.; Bradley, D. D. C.; Durrant, J. R. *J. Am. Chem. Soc.* **2008**, *130*, 3030.
(16) Koster, L. J. A.; Mihailetchi, V. D.; Blom, P. W. M. *Appl. Phys. Lett.* **2006**, *88*, 052104.
(17) Frost, J. M.; Cheynis, F.; Tuladhar, S. M.; Nelson, J. *Nano Lett.* **2006**, *6*, 1674.
(18) Hwang, I. W.; Soci, C.; Moses, D.; Zhu, Z. G.; Waller, D.; Gaudiana, R.; Brabec, C. J.; Heeger, A. J. *Adv. Mater.* **2007**, *19*, 2307.
(19) De, S.; Pascher, T.; Maiti, M.; Jespersen, K. G.; Kesti, T.; Zhang, F. L.; Inganas, O.; Yartsev, A.; Sundstrom, V. *J. Am. Chem. Soc.* **2007**, *129*, 8466.
(20) Westenhoff, S.; Howard, I. A.; Friend, R. H. *Phys. Rev. Lett.* **2008**, *101*, 016102.
(21) Tvingstedt, K.; Vandewal, K.; Gadisa, A.; Zhang, F. L.; Manca, J.; Inganas, O. *J. Am. Chem. Soc.* **2009**, *131*, 11819.
(22) Zhou, Y.; Tvingstedt, K.; Zhang, F.; Du, C.; Ni, W.-X.; Andersson, M. R.; Inganäs, O. *Adv. Funct. Mater.* **2009**, *19*, 3293.
(23) Vangeneugden, D. L.; Vanderzande, D. J. M.; Salbeck, J.; van Hal, P. A.; Janssen, R. A. J.; Hummelen, J. C.; Brabec, C. J.; Shaheen, S. E.; Sariciftci, N. S. *J. Phys. Chem. B* **2001**, *105*, 11106.
(24) Hallermann, M.; Haneder, S.; Da Como, E. *Appl. Phys. Lett.* **2008**, *93*, 053307.
(25) Ito, F.; Ikoma, T.; Akiyama, K.; Watanabe, A.; Tero-Kubota, S. *J. Phys. Chem. B* **2005**, *109*, 8707.
(26) Xu, Z. H.; Hu, B.; Howe, J. *J. Appl. Phys.* **2008**, *103*, 043909.
(27) Shakya, P.; Desai, P.; Kreouzis, T.; Gillin, W. P.; Tuladhar, S. M.; Ballantyne, A. M.; Nelson, J. *J. Phys.: Condens. Matter* **2008**, *20*, 452203.
(28) Ito, F.; Ikoma, T.; Akiyama, K.; Kobori, Y.; Tero-Kubota, S. *J. Am. Chem. Soc.* **2003**, *125*, 4722.
(29) Ogiwara, T.; Ikoma, T.; Akiyama, K.; Tero-Kubota, S. *Chem. Phys. Lett.* **2005**, *411*, 378.
(30) Xu, Z. H.; Hu, B. *Adv. Funct. Mater.* **2008**, *18*, 2611.
(31) Xu, Z. H.; Zang, H. D.; Hu, B. *Jom-Us* **2008**, *60*, 49.
(32) Frankevich, E. L.; Lymarev, A. A.; Sokolik, I.; Karasz, F. E.; Blumstengel, S.; Baughman, R. H.; Horhold, H. H. *Phys. Rev. B* **1992**, *46*, 9320.
(33) Frankevich, E.; Zakhidov, A.; Yoshino, K.; Maruyama, Y.; Yakushi, K. *Phys. Rev. B* **1996**, *53*, 4498.
(34) Veeraraghavan, G.; Nguyen, T. D.; Sheng, Y.; Mermer, O.; Wohlgenannt, M. *J. Phys.: Condens. Matter* **2007**, *19*, 036209.
(35) Tolstov, I. V.; Belov, A. V.; Kaplunov, M. G.; Yakuschenko, I. K.; Spitsina, N. G.; Triebel, M. M.; Frankevich, E. L. *J. Lumin.* **2005**, *112*, 368.
(36) Hu, B.; Yan, L. A.; Shao, M. *Adv. Mater.* **2009**, *21*, 1500.
(37) Geacintov, N. E.; Pope, M.; Fox, S. *J. Phys. Chem. Solids* **1970**, *31*, 1375.
(38) Steiner, U. E.; Ulrich, T. *Chem Rev* **1989**, *89*, 51.
(39) Onsager, L. *Phys. Rev.* **1938**, *54*, 554.
(40) Wohlgenannt, M.; Vardeny, Z. V. *J. Phys.: Condens. Matter* **2003**, *15*, R83.
(41) Schott, M.; Berrehar, J. *Mol. Cryst. Liq. Cryst.* **1973**, *20*, 13.
(42) Pope, M.; Burgos, J.; Wotherspoon, N. *Chem. Phys. Lett.* **1971**, *12*, 140.
(43) Hu, B.; Wu, Y. *Nat. Mater.* **2007**, *6*, 985.
(44) Doubleday, C.; Turro, N. J.; Wang, J. F. *Acc. Chem. Res.* **1989**, *22*, 199.
(45) Xu, Z. H.; Wu, Y.; Hu, B. *Appl. Phys. Lett.* **2006**, *89*, 131116.
(46) Baldo, M. A.; Adachi, C.; Forrest, S. R. *Phys. Rev. B* **2000**, *62*, 10967.
(47) Davis, A. H.; Bussmann, K. *J. Vac. Sci. Technol., A* **2004**, *22*, 1885.
(48) Ern, V.; Merrifie, R. E. *Phys. Rev. Lett.* **1968**, *21*, 609.
(49) Pope, M.; Swenberg, C. E. *Electronic processes in organic crystals and polymers*; 2nd edition; Oxford University Press: New York, 1999.
(50) Kalinowski, J.; Godlewski, J. *Chem. Phys. Lett.* **1975**, *36*, 345.
(51) Kalinowski, J.; Szmytkowski, J. D.; Stampor, W. *Chem. Phys. Lett.* **2003**, *378*, 380.
(52) Tajima, H.; Miyakawa, M.; Isozaki, H.; Yasui, M.; Suzuki, N.; Matsuda, M. *Synth. Met.,* i.
(53) Wu, Z.; Kumagai, N.; Yoshimura, M. *Chem. Mater.* **2000**, *12*, 3356.
(54) Mandal, S.; Goswami, M. L. N.; Das, K.; Dhar, A.; Ray, S. K. *Thin Solid Films* **2008**, *516*, 8702.
(55) Lide, D. R. CRC Handbook of Chemistry and Physics; 89th edition. 2008−2009, 12−52.
(56) Sun, Z. H.; Wang, C. X.; Yang, J. X.; Zhao, B.; Lombardi, J. R. *J. Phys. Chem. C* **2008**, *112*, 6093.
(57) Clarke, T. M.; Ballantyne, A. M.; Nelson, J.; Bradley, D. D. C.; Durrant, J. R. *Adv. Funct. Mater.* **2008**, *18*, 4029.
(58) Yang, X. N.; Loos, J.; Veenstra, S. C.; Verhees, W. J. H.; Wienk, M. M.; Kroon, J. M.; Michels, M. A. J.; Janssen, R. A. J. *Nano Lett.* **2005**, *5*, 579.
(59) Ma, W. L.; Yang, C. Y.; Gong, X.; Lee, K.; Heeger, A. J. *Adv. Funct. Mater.* **2005**, *15*, 1617.
(60) Erb, T.; Zhokhavets, U.; Gobsch, G.; Raleva, S.; Stuhn, B.; Schilinsky, P.; Waldauf, C.; Brabec, C. J. *Adv. Funct. Mater.* **2005**, *15*, 1193.
(61) Mihailetchi, V. D.; Xie, H. X.; de Boer, B.; Koster, L. J. A.; Blom, P. W. M. *Adv. Funct. Mater.* **2006**, *16*, 699.
(62) Savenije, T. J.; Kroeze, J. E.; Yang, X. N.; Loos, J. *Adv. Funct. Mater.* **2005**, *15*, 1260.
(63) Kim, Y.; Choulis, S.; Nelson, J.; Bradley, D.; Cook, S.; Durrant, J. *J. Mater. Sci.* **2005**, *40*, 1371.
(64) Li, G.; Shrotriya, V.; Yao, Y.; Yang, Y. *J. Appl. Phys.* **2005**, *98*, 043704.
(65) Kim, Y.; Choulis, S. A.; Nelson, J.; Bradley, D. D. C.; Cook, S.; Durrant, J. R. *Appl. Phys. Lett.* **2005**, *86*, 063502.
(66) Reyes-Reyes, M.; Kim, K.; Carroll, D. L. *Appl. Phys. Lett.* **2005**, *87*, 083506.
(67) Nguyen, L. H.; Hoppe, H.; Erb, T.; Gunes, S.; Gobsch, G.; Sariciftci, N. S. *Adv. Funct. Mater.* **2007**, *17*, 1071.
(68) Dante, M.; Peet, J.; Nguyen, T. Q. *J. Phys. Chem. C* **2008**, *112*, 7241.
(69) Chirvase, D.; Parisi, J.; Hummelen, J. C.; Dyakonov, V. *Nanotechnology* **2004**, *15*, 1317.
(70) Jo, J.; Kim, S. S.; Na, S. I.; Yu, B. K.; Kim, D. Y. *Adv. Funct. Mater.* **2009**, *19*, 866.
(71) Taneja, P.; Ayyub, P.; Chandra, R. *Phys. Rev. B* **2002**, *65*, 245412.
(72) Ou, Z. M.; Yao, H.; Kimura, K. *Chem. Soc. Jpn.* **2007**, *80*, 295.
(73) Vandewal, K.; Tvingstedt, K.; Gadisa, A.; Inganas, O.; Manca, J. V. *Nat. Mater.* **2009**, *8*, 904.

JP100241G